This is a preprint, the final version is subject to change, of the American Mineralogist (MSA)
Cite as Authors (Year) Title. American Mineralogist, in press.
(DOI will not work until issue is live.) DOI: http://dx.doi.org/10.2138/am-2016-5621

REVISION 1

A new experimental approach to study fluid – rock equilibria at the slab-mantle interface based on the synthetic fluid inclusion technique

ALEXANDRA TSAY [1,2,*], ZOLTAN ZAJACZ [1], PETER ULMER [2], MARKUS WAELLE [2] AND CARMEN SANCHEZ-VALLE[3]

[1]Department of Earth Sciences, University of Toronto, 22 Russell St., M5S 3B1, Toronto, Canada

[2] Institute of Geochemistry and Petrology, ETH Zurich, Clausiusstr. 25, 8092 Zurich, Switzerland

[3] Institut f. Mineralogie, Universität Münster, Corrensstr. 24, 48149 Münster, Germany

Abstract

The role of high-pressure aqueous fluids in mass transfer processes during slab dehydration has been long time recognized. However, the quantitative assessment of their material transport capacity in complex natural systems remains poorly understood, mainly as a consequence of their unquenchable nature and current experimental limitations. A new experimental approach has been developed to investigate complex fluid – rock equilibria at high pressure and temperature conditions relevant for slab dehydration processes. Aqueous fluids pre-equilibrated with high pressure mineral assemblages were sampled at run conditions in the form of synthetic fluid inclusions (SFI) in quartz and subsequently analyzed by laser-ablation ICPMS (LA-ICPMS). The main innovation introduced in the experiments is that the quartz crystal was fractured in-situ during the run only after chemical equilibrium between phases has been achieved, thus allowing the entrapment of fluid inclusions that sample true equilibrium compositions. An efficient fracturing of quartz at high pressure and temperature conditions was achieved by crossing the α-quartz – coesite reaction boundary, which occurs at pressures of the sub-arc slab - mantle

interface. An experimental methodology has been developed to implement this strategy and experiments in the eclogite - water system were conducted to demonstrate the feasibility and advantage of the method. The results demonstrate that secondary fluid inclusions formed early in pre-fractured quartz are systematically diluted compared to secondary inclusions formed after in-situ fracturing of quartz, particularly for elements such as Sr, Zr, Nb, Ti and Mg. These observations demonstrate that early entrapment of fluids in pre-fractured quartz do not represent equilibrium fluids at high pressure-temperature conditions.

Keywords: Subduction zone, magma, slab dehydration, high-pressure fluids, synthetic fluid inclusions

Introduction

Aqueous fluids along with hydrous melts and supercritical liquids are considered as the transport agents responsible for large scale mass transfer from the subducting slab to the mantle wedge (e.g. Manning, 2004; Poli and Schmidt, 2002; Scambelluri and Philippot, 2001; Ulmer, 2001). However, it remains unclear which of these mobile phases is responsible for the transfer of slab-derived components that metasomatize the mantle wedge, ultimately leading to the characteristic trace element signature of arc magmas. Hydrous silicate melts have received the most attention in terms of mineral solubility and trace element partitioning studies because they can be sampled by quenching them to glasses and subsequently analyzed by a number of techniques. Numerous experimental studies have reported the composition of hydrous silicate melts in equilibrium with relevant mineral assemblages (e.g. Brenan et al., 1995a; Klemme et al., 2002, 2005; Prowatke and Klemme, 2006; Hermann and Rubatto, 2009; Hermann and Spandler, 2008; Klimm et al., 2008; Skora and Blundy, 2012; Spandler and Pirard, 2013), and many authors consider melts as the main transport agent. The available information on the composition

of aqueous fluids is much scarcer as they cannot be quenched and experiments suited to determine their composition at high pressure (*P*) and temperature (*T*) remain challenging.

One of the first experimental approaches established to determine the solubility of minerals in high *P* - *T* aqueous fluids is the weight-loss technique. This technique has been well proven on systems that dissolve congruently, such as calcite/quartz/rutile - H_2O (e.g. Caciagli and Manning, 2003; Manning, 1994; Tropper and Manning, 2005). However, its application is limited in multi-component systems, which involve incongruent dissolution of the mineral phases, as well as in mineral solubility studies at trace concentration levels or in fluid/mineral partitioning studies. The unquenchable nature of aqueous phases has thus required the development of original experimental approaches to characterize in-situ the chemical composition and/or structure of aqueous fluids and hydrous melts at conditions relevant for subduction zones. For instance, approaches employing diamond anvil cells (DAC) in conjunction with synchrotron X-rays have provided new insights into the solubility of minerals and on the partitioning and speciation of trace elements at high *P* – *T* conditions (e.g., Basset et al., 1993; Mayanovic et al., 2002; Sanchez-Valle et al. 2003; Manning et al., 2008; Bureau et al., 2010; Wilke et al., 2012; Louvel et al., 2013). However, the application of this technique is also limited to: 1) relatively simple chemical systems, i.e. monomineralic or with melting temperatures below 950 °C, that correspond to the typical operation conditions of externally heated DACs, and 2) trace elements whose absorption and emission energies fall in the range of transparency of the diamond window of the DAC (> 4 keV, Basset et al., 2000; Sanchez-Valle, 2013). This last constraint precludes in-situ investigations of important geochemical elements in subduction zone fluids, including Si, Al, S, Cl, Na or Mg. Much progress in the analysis of fluid compositions in complex chemical systems has been achieved by applying the diamond-trap technique, where equilibrium high pressure fluids are preserved between the grains of a porous diamond layer placed in contact with

the mineral assemblages. Though the approach was originally proposed in 1980 (Ryabchikov and Boettcher 1980; Kushiro and Hirose, 1992), recent developments on the analytical setup significantly improved and widened the applications of this method to volatile-rich systems (Kessel et al., 2004; Aerts et al., 2010). In particular, the introduction of cryogenic LA-ICPMS analysis, where the hydrous phase is frozen in between the diamond grains until ablated with the laser, minimizes any element losses and allows the investigation of aqueous fluids, hydrous melts and supercritical liquids in equilibrium with complex mineral assemblages (e.g., Kessel et al., 2005a; Kessel et al., 2005b; Stalder et al., 1998). However, using this approach, special care has to be taken to avoid potential fluid contamination by mineral phases that can precipitate in the diamond layer. Some of the problems can be overcome by employing a rocking piston cylinder apparatus, which allows rotating the experimental assembly periodically by 180 degrees during the experiment, to promote equilibration and minimize the precipitation of solid phases in the diamond layer (Schmidt and Ulmer, 2004). Yet, such an apparatus is available only in a few experimental laboratories worldwide. An alternative approach to investigate high pressure fluids is the synthetic fluid inclusion (SFI) technique, which minimizes potential fluid contamination with the solid, although only quartz saturated systems can be investigated.

The SFI technique has been widely applied over the last decades to study natural fluid systems at various upper to lower crustal conditions (Bodnar, 1987). Pre-fracturing of the host mineral by a thermal shock near the α - β quartz transition, associated with rapid volume change, is a common and effective way to form fluid inclusions during the experiment (Sterner and Bodnar, 1984). The basic idea of this method is that the fractures in quartz crystal heal during the experiment by dissolution - reprecipitation to minimize surface energy, **forming the so-called secondary fluid inclusions. Quartz is the most common host for SFI, although other silicate minerals such as olivine have also been employed (Bali et al., 2013).** During this process,

93 droplets of fluids are trapped in the fractures and are preserved as fluid inclusions which permit
94 sampling of the fluid at run *T* and *P*. This approach has also been applied to investigate element
95 mobilities from subducted sediments by healing the fractures in quartz at high *P* and *T* (Spandler
96 et al., 2007). However, in this case, one needs to consider the different time scales required for
97 fluid inclusion formation, i.e. healing of the fractures, and that of equilibration that is
98 comparatively slow. If the fractures heal before the mineral assemblage and fluid phase
99 equilibrate, the composition of the fluid inclusions does not represent that of the equilibrated
100 fluid. In principle, the higher the solubility of quartz is at run conditions, the faster the fractures
101 are expected to heal. As quartz solubilities in aqueous fluids in the *P* - *T* range relevant for slab
102 dehydration are rather high (Manning, 1994), such premature fracture healing is expected.
103 Previously, this issue has been overcome in rapid quench pressure vessel assemblies, which allow
104 the fracturing of quartz inside the pressure vessel during the experiment. Rapid quenching and
105 reheating of quartz at any time during the experiment by moving the capsule between the hot and
106 cold end of the vessel allows sufficient time for equilibration before the fluid inclusions form
107 (e.g., Zajacz et al., 2010). However, this experimental setup covers only the pressure range of the
108 upper crust, where the α to β quartz transition takes place. For high pressure solubility
109 experiments in a piston-cylinder apparatus, an alternative approach based on the formation of
110 primary fluid inclusions during quartz overgrowth has been applied. In this case, thermal
111 gradients along the capsule (< 15 °C) promote dissolution of quartz in the hot part and
112 precipitation of new quartz in the cooler part of the capsule, allowing primary inclusions to be
113 trapped. Yet, this particular design is appropriate for solubility studies when the equilibrium
114 between the solid and the fluid can be attained relatively fast, e.g. within a few hours to days,
115 which corresponds to the time required for quartz dissolution and reprecipitation at 800 °C (e.g.
116 Bali et al., 2011; Bali et al., 2012; Tsay et al., 2014). However, in complex multi-component

117 systems involving mineral phases characterized by low element diffusivities, longer run durations
118 may be required and this approach is not suitable.

119 In this contribution, we developed a new experimental approach to improve the SFI
120 technique and to extend its application to complex fluid – rock equilibria at sub-arc slab – mantle
121 interface conditions. The essential progress is that we provide control on the time of fluid
122 inclusion formation. After equilibration of the phases in the experiment, the host mineral quartz is
123 in-situ fractured at the desired point in time so that the fluid phase can be sampled in the form of
124 SFI at run conditions. This new approach was originally developed to investigate allanite
125 solubility as well as major and trace element compositions in aqueous fluids in equilibrium with
126 an eclogitic mineral assemblage. Preliminary results on selected major/trace element (Na, Mg, Ti,
127 REE, Zr, Sr, Ba and Nb) solubility at 700 - 800 °C and 2.5 - 2.6 GPa are presented here to
128 demonstrate the progress and feasibility of the method.

129 **Experimental methods**

130 **Experimental strategy and procedure**

131 A prerequisite in the investigation of mineral solubility or element partitioning between the
132 solid and fluid phases is the achievement of equilibrium, which is largely controlled by the
133 slowest element diffusivities. Equilibration time may hence require relatively long run durations,
134 particularly in the case of element partitioning experiments. To satisfy this requirement, the
135 strategy was to form a network of fractures in quartz during the experiment but after the solid and
136 fluid phases have equilibrated. However, the attempts to in-situ fracture the host crystal by
137 sudden quenching and reheating during the experiment within the stability field of α-quartz was
138 not successful (e.g., # 51). This indicates that the thermal shock alone does not induce significant
139 fracturing of quartz at high *P* as observed in the lower/atmospheric *P* range across the α – β

quartz transition. Therefore, to implement this technique at conditions of the sub-arc slab - mantle interface, the *P* and *T* of the experiment were cycled across the α - quartz ↔ coesite transition boundary (**e.g. Bose and Ganguly, 1995**), as shown schematically in Figure 1.

In practice, the following procedure is applied for the entrapment of the fluid phase (Fig. 1): (1) the solid and fluid phases are equilibrated at the nominal *P* and *T*; (2) the sample is compressed across the α-quartz – coesite phase boundary; (3) the sample is quenched down to ~ 300 °C to induce a sudden decompression, which is possible due to relatively large amount of aqueous fluid in the experimental charge and the thermal expansion/contraction of the entire piston cylinder assembly; (4) the sample is reheated and brought back to the equilibration *P* and *T* conditions, where the system is maintained to form SFI by healing the fractures in quartz. Each of the steps has been tested in order to optimize the procedure. For example, the compression step (2) lasted for a few hours to let the assembly transmit the pressure and allow the α-quartz to convert to coesite. **We intentionally overstepped the phase boundary conditions by 0.7 – 0.8 GPa to achieve relatively fast the phase transformation. This is not expected to greatly affect the composition of the fluid as the estimated change in fluid density, which controls the extend of mineral solubility (e.g., Manning, 1994), is only ~ 0.06 at 800 °C and ~ 0.07 at 700 °C over the investigated pressure interval (Churakov and Gottschalk, 2003). Furthermore, the duration of the compression step was relatively short to prevent re-equilibration of the system at higher *P*.** On the other hand, fast quenching and reheating (steps 3 – 4, typically few seconds) was applied to bring the system to equilibrium run conditions. The purpose of quenching, instead of simply bringing the sample back to the equilibration *P*, was to ensure relatively fast decompression and the transition of coesite to α-quartz, so that the fluid inclusions (FI) of the right density could form. The time allowed for the formation of FI varied, depending on the *T* of the experiment. For example, at 800 °C, many fractures have healed and

contained FI after ~ 2 days, whereas at 590 °C the system was maintained at run conditions for ~ 6 days after fracturing. Furthermore, the success of the suggested procedure depended on many other aspects, such as capsule design, solid/fluid mass ratio as well as the type of pressure transmitting media as discussed in the following sections. **Three additional experiments were performed with pre-fractured quartz (# 69, 93 and 95) to demonstrate the requirement of in-situ fracturing to sample representative fluid compositions. The experiments were run at the same *P – T* conditions as the in-situ fractured experiments (# 63 and 62) to allow direct comparison.**

All experiments have been conducted in an end-loaded Boyd and England type piston-cylinder apparatus. A friction correction of – 10% was applied to the nominal pressure for MgO/BN/Pyrex – graphite - Pyrex - Talc assemblies and – 5% for a BN – graphite - NaCl assembly (Fig. 2). Pressure was calibrated against the quartz – coesite transition at 1000 °C and 3.07 GPa (Bose and Ganguly, 1995) and the univariant reaction fayalite + quartz = orthoferrosilite at 1000 °C and 1.41 GPa (Bohlen et al., 1980). Temperature was determined from the reading of a type B thermocouple ($Pt_{94}Rh_6$ – $Pt_{70}Rh_{30}$) with a precision of about 2 – 3 °C.

Sample preparation

A natural eclogite sample from the Nordfjord area of southwestern Norway was used as starting material for the experiments. The rock sample mainly consists of pyrope - almandine garnet and omphacitic pyroxene with some amphibole, quartz and accessory rutile. In general, two kinds of starting materials were prepared for the experiments. Initially, the rock sample was finely crushed to ~ 7 – 10 µm grain size and used for the series of reconnaissance experiments. A natural gem quality allanite crystal from Trimouns Talc mine (France) was also crushed and ~ 3 wt% were added to the eclogite powder. A solid/fluid mass ratio of ~ 1 resulted in significant

187 changes in mineral composition during the experiment. In particular, the omphacite was
188 transformed into diopsidic clinopyroxene and orthopyroxene (# 50, 51, Table 2). To avoid this
189 and to preserve the Na and Al – rich eclogitic pyroxene in equilibrium with aqueous fluid, the
190 starting composition was modified by changing the phase modes and adding natural kyanite. The
191 second starting material, referred to as "II" in Tables 1 and 2, contained ~ 67 wt% of omphacite,
192 ~ 19 wt% of garnet, ~ 9 wt% of kyanite, ~ 3 wt% of allanite, ~ 1wt% of zircon and ~ 1 wt% of
193 rutile. Garnet and pyroxene were handpicked from the same eclogite sample. All phases were
194 finely crushed and thoroughly mixed in the agate mortar. The solid/fluid ratio was also increased
195 up to 1.7 - 2 to minimize the alteration of the phases in the solid residue. In the following
196 experiment, orthopyroxene did not form, but all omphacite was converted into diopside (# 52).
197 Therefore, in all the subsequent experiments, a synthetic albite glass was added to the fluid. The
198 equilibrium concentrations of Na in the fluid and the diopsidic clinopyroxene in the Na depleted
199 experiment (# 52, ~ 1.6 wt% of Na in the fluid, ~ 1.78 wt% of Na_2O in the pyroxene) were used
200 to obtain an initial estimate for Na concentration in the fluid that would be in equilibrium with
201 omphacite. At 800 °C, ~ 3 - 6 wt% of Na relative to the total weight of the fluid was added in the
202 form of albite glass, whereas at 700 °C, this quantity was reduced to ~ 1.5 - 3 wt% of Na (or
203 X_{Albite} ~ 0.02 – 0.01, Table 2). In all experiments with albite glass, omphacite was preserved as a
204 stable clinopyroxene with Na_2O concentration of 4 to 7 wt%.

205 The bulk composition of both starting materials was determined by fusing mineral mixtures
206 in a platinum crucible at ~ 1400 °C for 2 hours. The resulting glasses were analyzed by electron
207 microprobe and LA-ICPMS. The composition of the mineral phases and bulk composition of the
208 starting materials are provided in Table 1. Pure H_2O was used as solvent for all experiments.
209 Trace amounts (~ 500 ppm) of Rb and Cs were added to the solvent in the form of bromides
210 (Alfa Aesar, 99.9 % purity) and served as internal standards for LA-ICPMS analyses of SFI.

Both Cs and Rb are expected to behave as highly incompatible elements in K-free (mica-free) eclogites, and therefore preferentially partition into the fluid phase. A similar approach has been used to analyze the composition of fluids by LA-ICPMS in diamond-trap experiments (Kessel et al., 2004).

Capsule preparation and the choice of assembly material

A double capsule technique similar to the approach of Spandler et al (2007) has been applied (Fig. 3). The internal capsule containing the starting material was welded on one side and crimped on the other side, while the external capsule was loaded with a piece of quartz, the internal capsule, aqueous fluid (~ 10 – 12 µl) and welded on both sides. The employment of the internal capsule served to prevent the starting material from spreading in the aqueous fluid and to avoid contamination of SFI by heterogeneously entrapped mineral fragments. However, a problem encountered here was that the access of the fluid to the mineral assemblage was blocked during the experiment, which may have happened before the solid and fluid equilibrated. This, in turn, may result in erroneously low element concentrations in the fluid phase as demonstrated later in section "experimental drawbacks". To ensure the long term fluid access to the solid, two different approaches have been applied. The idea of the first approach was to place a layer of poorly reactive material on the top and the bottom of the internal capsule and to pierce the capsule on both sides so that the fluid can be flushed by infiltration through these two layers (Fig. 3a). In this way, the reaction front was displaced and the fluid/solid interface area was significantly increased. Zirconia spheres (ZrO_2) or finely crushed natural zircon were used as infiltrating medium. **In the case of ZrO_2 layers, zircon extensively precipitated around the spheres since the fluid in all experiments was quartz saturated (Fig. 4a). Although the solid residue in these experiments appeared to be extensively reacted, the newly grown zircon**

234 **phase most likely affects the bulk solid – fluid equilibrium during the experiment. In the**
235 **subsequent experiments, the layers of ZrO_2 were substituted by natural zircon (Fig. 4b).**
236 **However in this case, the increase in modal proportion of zircon may partly control the**
237 **bulk partition coefficients of the HREE (e.g. $D_{HREE}^{Zc/melt} \sim 13 - 500$, Fujimaki, 1986; Thomas et**
238 **al., 2002), because zircon is no longer an accessory phase but a major constituent of the**
239 **rock.** Considering all the above mentioned uncertainties and potential difficulties, the second
240 approach consisted of piercing the internal capsule and adding a few relatively large crystal
241 fragments (> 100 μm) of accessory phases (allanite, rutile and zircon) and garnet to the external
242 capsule to ensure their contact with the fluid phase throughout the experiment (Fig. 3b). The
243 reason for using large crystal fragments was to prevent them from being trapped in the SFI and to
244 be able to recover them after the experiment for electron microprobe examination. The solid
245 residue in these experiments did not entirely react, showing some patches of less-reacted material
246 along the inner capsule. However, all the phases did show nearly homogeneous reaction rims
247 completely surrounding the unreacted cores, e.g. relatively Na-rich omphacite rim around Na-
248 poorer starting omphacite, REE – depleted allanite or zoisite rim around allanite. In the case of
249 garnets, a clear reaction rim was formed in the experiments at 800 °C, whereas no significant
250 compositional changes were observed at 700 °C (Fig. 4c-d).

251 All the experiments have been conducted in gold (Au) capsules. The internal capsule was
252 usually about 7 - 8 mm long and 2 mm (OD) in diameter. Quartz cores of cylindrical shape and ~
253 1.8 mm in diameter were prepared for the experiments. The external capsule was about 11.3 to
254 14.6 mm long and 4 mm (OD) in diameter. Runs # 69, 93 and 95 were performed with a piece of
255 quartz pre-fractured before the experiment. In experiment 69, a small piece of pristine quartz was
256 also added to initiate the formation of primary FI (Fig. 3c).

Another important aspect was the choice of assembly material along with the solid/fluid mass ratio. The right combination of both ensured fracturing of quartz as well as maintaining the integrity of the capsule upon sudden cooling and decompression accompanied with rapid fluid volume changes. Different types of assembly have been tested: (a) BN or MgO – Pyrex – Talc; (b) Pyrex – Pyrex – Talc; (c) BN – NaCl (Fig. 2). A summary of the experiments performed using different types of assembly and other experimental details are shown in Table 2. A set of reconnaissance experiments was performed using assembly (a) employing either BN or MgO, as material surrounding the capsule (Fig. 2a). The solid/fluid ratio in those experiments was close to 1. In the experiments with BN, the recovered capsule was found heavily deformed and did not contain any fluid. The inspection of the recovered quartz showed neither fluid inclusions nor any signs of fracturing (# 48, 49). In the subsequent experiments with MgO, the capsule shape was better preserved and the fluid was preserved in the capsule during the experiment; however, the fracturing of quartz and the phase transition was not always efficient. One experiment did show many FI along healed fractures (# 50) and the quartz converted to coesite during the experiment, which was later identified by Raman spectroscopy. This suggests that the host mineral was likely fractured during the quartz – coesite phase transition; the transition back to α-quartz did, however, not occur and the FI formed in the coesite stability field. In the following experiment with the same type of assembly, the host mineral did not fracture and only primary FI formed on one side of the quartz core (# 51), suggesting that the quartz – coesite phase boundary was never crossed during the experiment. In the experiments performed using the third type of assembly (Fig. 2b), different solid/fluid ratios were tested. In particular, the experiment with a solid/fluid ratio of ~ 1.7 showed extensive fracturing of the host mineral and many FI formed (# 52), whereas in the experiment with a solid/fluid ratio of ~ 2 quartz did not fracture but contained a network of primary FI in the overgrowth zone (Fig. 5a, # 54). **Besides, a relatively high amount**

of albite glass (X_{Albite} ~ 0.04) has been added in the later experiment with the purpose of preserving omphacite. Thus, taking into account the increased solid/fluid ratio and the addition of albite glass, it is possible that the fluid was significantly more solute-rich and the water activity was lower in this experiment. This, in turn, may have reduced the catalytic effect of water on the kinetics of α-quartz – coesite phase transition and, therefore, prevent the fracturing of quartz. Therefore, the ratio of ~ 1.7 was considered as an optimum for this bulk composition and used in all the subsequent experiments. However, the assembly type was found to be insufficient for fracturing at lower *T* of 700 °C. The forth type of assembly was particularly different from the previous ones, as there was neither Pyrex nor talc involved, but a salt (NaCl) cell surrounding the graphite furnace (Fig. 2c). All the experiments performed with this type of assembly were successful in terms of fracturing of quartz and the formation of SFI, including the experiments at lower *T*. The oxygen fugacity was not explicitly controlled during the experiment, but the use of various assembly types may have imposed somewhat different redox conditions. For example, the redox sensitive Eu showed a negative anomaly in the experiments with BN - NaCl assembly (# 62, Fig. 6), whereas in the experiment with Pyrex – talc the anomaly was less pronounced (# 52, 54, Fig. 6). This observation suggests that relatively more reducing conditions were imposed by the BN – NaCl assembly, which led to reduction of Eu from 3+ to 2+.

Run products preparation and analytical methods

After the experiment, the capsule was weighted to check for fluid leaks, then gently pierced and opened to ensure minimum damage to the internal capsule and quartz. In all the successful experiments, fluid was present upon opening the capsule. The recovered internal capsule was first impregnated in epoxy and dried overnight. Then the entire capsule was mounted in epoxy and

304 exposed by polishing about half way through. If required, the procedure of impregnating and
305 polishing was repeated until the surface of the mineral phases was well polished for electron
306 microprobe analysis. Quartz was usually recovered in fragments that were mounted on a glass
307 support using UV-cured epoxy to avoid any heating and prevent decrepitation of FI. Selected
308 quartz fragments were polished and prepared for the LA-ICPMS analysis of FI.

309 A detailed chemical and textural analysis of the run products has been performed on a JEOL
310 JXA-8200 electron microprobe at ETH Zurich. A 15 kV acceleration voltage and 20 s of peak
311 counting time were applied. All mineral phases were analyzed with a focused beam and 20 nA of
312 beam current, whereas for glass analysis a 30 μm beam diameter and 7 nA of beam current were
313 used. The peak counting time for Na in glasses was reduced to 10 s. Major elements were
314 standardized using wollastonite (Si and Ca), jadeite (Na), corundum (Al), forsterite (Mg), fayalite
315 (Fe), K-feldspar (K), chromite (Cr), pyrolusite (Mn) and rutile (Ti). Most of the rare-earth
316 elements (La, Pr, Nd, Sm, Gd) were standardized using synthetic REE-aluminates ($REEAlO_3$) but
317 CeO_2 was used for Ce. Peak and background positions for REE were selected to avoid spectral
318 overlaps based on qualitative scans on the natural allanite crystal. The SFI were analyzed by LA-
319 ICPMS at ETH Zurich with a laser ablation system described in Heinrich et al. (2003). The NIST
320 SRM 610 glass was used as external standard and the known concentrations of Cs and Rb in the
321 fluid were used as internal standards to quantify all other analytes. The laser spot size was
322 manually increased during ablation with an iris aperture to exceed the size of FI by the end of the
323 ablation (Gunther and Heinrich, 1999). Small amounts of H_2 [5 ml/min] were added to the He
324 carrier gas [1.15 l/min] to improve the detection limits and the precision of the trace element
325 analysis (Guillong and Heinrich, 2007).

326 **Results and discussion**

Experimental drawbacks

A series of reconnaissance experiments, devoted to optimizing the starting material and the experimental setup (# 48 – 51), are not included in the discussion. But some of the experimental problems mentioned before are illustrated here. For example, the formation of primary FI or a limited fluid access to the solid residue during the experiment, both of which resulted in lower REE concentrations in the fluid phase. In particular, in experiment 54, with solid/fluid ratio of ~ 2, quartz did not undergo fracturing but a group of primary FI formed on one end of the quartz core (Fig. 5a). Conversely, in experiment 58, with a reduced solid/fluid ratio of ~ 1.7, quartz was fractured and both primary and secondary FI formed (Fig. 5b). However, the examination of run products revealed poorly reacted solid residues, particularly in experiment 58, and the composition of FI in both of the experiments was rather diluted compared to the previous experiments (e.g. # 52, Fig. 6a). Altogether, these observations suggest a relatively early formation of FI and, probably, limited solid – fluid interaction during the experiment. Another important detail is the composition of the starting fluids, which in both the experiments contained ~ 6 wt% of Na (X_{Albite} ~ 0.04). Consequently, a relatively high albite content in the starting fluids most likely promoted a relatively fast quartz overgrowth and formation of FI as well as the observed extensive precipitation of Na- rich omphacite around the holes pierced into the internal capsule, so that the fluid access was blocked to the rest of the mineral assemblage at a certain stage during the experiment. Therefore, the FI in both experiments do not represent fluids in equilibrium with the solid residue. **Similar problems have been encountered in the series of experiments at 700 °C. For example, experiment 56 at 700 °C is equivalent to experiment 58 at 800 °C in terms of bulk composition and relatively high amount of albite glass added to the starting fluid, i.e. X_{Albite} ~ 0.02 (Table 2). Run products in experiment 56 also revealed poor solid - fluid interaction and an abundant precipitation of high Na and Al**

clinopyroxene. It is interesting to note that independent from temperature differences in these two experiments (# 56 and 58), the concentration level and the pattern of REE are rather similar (Fig. 6b). On the other hand, the REE pattern from experiments 52, 54 and 62 at 800 °C resembles the relative abundances of REE in allanite (Fig. 6a,b), which is the main source of LREE in the experiment. As for experiments 56 and 58, most notable deviation from the allanite-imposed pattern is the La/Ce ratio, which appears to be reversed in these two experiments, i.e. $(La/Ce)_{All} \sim 0.45$ vs. $(La/Ce)_{fluid} \sim 1.32$ and ~ 4.66 in experiments 58 and 56, respectively. Though the origin of the reversal of the La/Ce ratio and the limited effect of *T* on element concentrations in these experiments (# 56 and 58) are unclear, it may relate to a common problem of limited solid – fluid interaction, which was mainly controlled by the rate of clinopyroxene precipitation. Note that unlike in experiment 54 (Fig. 6a), quartz was in-situ fractured in these two experiments and, therefore, the formation of FI was relatively delayed, whereas in experiment 54 only primary FI have formed. In the subsequent experiments, the amount of albite glass was reduced to ~ 3 wt% of Na ($X_{Albite} \sim 0.02$) at 800 °C (# 62) and to ~ 1.5 wt.% of Na ($X_{Albite} \sim 0.01$) at 700 °C (# 63), as well as the fluid access to all the mineral phases was improved by the use of a modified capsule arrangement (Fig. 3b). The amount of albite glass was decreased in experiment at 700 °C as lower solubility of sodium-aluminosilicate component in the fluid is expected at lower *T*. This resulted in significantly higher REE concentrations in the fluid at 800 °C (# 62, Fig. 6a) and in similar concentration level but clearly allanite-imposed REE pattern (e.g. La/Ce ~ 0.46) at 700 °C (# 63, Fig. 6b). Despite the reduced albite glass content, omphacite with ~ 4 – 7 wt% of Na_2O was still a stable phase in experiments 62 and 63.

Comparison between ex-situ and in-situ fracturing of quartz

To illustrate the difference between ex-situ and in-situ fracturing of quartz on the composition of FI, we compare the results of experiments 69, 93 and 95 conducted with quartz pre-fractured before the experiment and those from experiment 63 and 62 performed with in-situ fracturing of quartz at identical *P* - *T* conditions. **In total, two runs (# 69 and 95) with pre-fractured quartz were conducted at 700 °C and one run (# 93) at 800 °C. In experiment 69, a pre-fractured quartz was loaded together with a pristine quartz (Fig. 3c), whereas in experiments 95 and 93, only a pre-fractured quartz was present. Run duration of ~ 48 hours was sufficient to heal the fractures in quartz and to form a large number of secondary FI in experiments 95 and 93. Experiment 69 was run for a longer duration, ~ 117 hours, to ensure the formation of primary FI.** Both primary and secondary FI could be distinguished by visual examination before LA-ICPMS analysis. A general observation was that the primary FI are often found in a group of relatively large (up to ~ 100 μm), negative crystal shaped and oriented inclusions. Instead, the secondary FI are rather small (~ 10 – 50 μm), rounded in shape and distributed on a trail/plane inside the quartz crystal, which may be randomly oriented. The primary inclusions, in turn, typically form along the growth front of the quartz crystal. An example of the secondary FI trail from experiment 69 is shown in Figure 5d. The inclusions in experiments 63 and 95 at 700 °C as well as in 62 and 93 at 800 °C were represented by secondary FI of rounded shape and ~ 10 – 30 μm size (Fig. 5c,d).

The results of experiments at 700 °C are presented in Figure 7. The concentration of Sr in the fluid reflects the most representative variation between the experiments; therefore other elements, such as Ba, Zr, Nb, Ti, Na and Mg, were plotted as a function of the Sr content. The analysis of primary FI from experiment 69 and secondary FI from experiments 69 and 95 indicated two distinct compositional groups. The group of secondary FI displays the most diluted fluid composition for all elements except for Na. The low

elemental concentrations in these FI mostly reflect a premature healing of the fractures, which likely started in early stages of the experiment. This may also be the reason for relatively elevated Na concentrations as the early trapped fluid may have been super saturated in the presence of metastable albite glass. Indeed the starting omphacite had lower Na concentrations than the overgrowth rims, demonstrating that Na was extracted from the fluid during the precipitation of newly grown omphacite. Alternatively, the group of primary FI displays a range of concentrations either close to composition of the secondary FI formed by ex-situ (# 69, 95) fracturing of quartz, e.g. Zr, Na and Mg, or a series of intermediate compositions, e.g. Sr, Ti and Nb. Finally, the secondary FI formed by in-situ fracturing in experiment 63 showed the highest concentrations for all the elements, except for Na, and are considered to represent the composition closest to fluids in equilibrium with eclogite. Barium was the only element for which the concentrations in the primary inclusions reached the fluid composition from experiment 63. This suggests that the primary FI could potentially sample equilibrium fluid compositions with respect to some element concentrations; however, special care has to be taken to recover the outermost growth zone of quartz re-precipitated during the experiment and to analyze the FI only from this zone, as they are the most representative for equilibrated fluid composition. This, in turn, may be rather difficult to achieve if the quartz core is recovered from the capsule in fragments, and the preparation and analysis of FI may require a special handling. Moreover, the total number of FI that could be analyzed is strongly reduced. Most of these difficulties have been overcome in the case of in-situ fracturing of quartz. For example, many FI form simultaneously throughout the quartz crystal, which makes the preparation for the analysis less demanding and a large number of FI can be analyzed, hence improving the quantification.

The results of experiments at 800 °C are shown in Figures 8 and 9. In this case, only secondary FI formed by ex-situ (# 93) and in-situ (# 62) fracturing of quartz are compared. The results reveal even more pronounced difference between ex-situ and in-situ fracturing of quartz, confirming that the fluids trapped in pre-fractured quartz are significantly more diluted in trace elements such as Sr, Ba, Zr and Nb (Fig. 8). Moreover, most of the major elements, e.g. Al, Ca, Mg, Fe and Ti, also show significantly lower concentrations in FI formed by ex-situ fracturing of quartz (Fig. 9a). Conversely, the concentrations of LREE and to a lesser extent that of Na, are lower in FI formed by in-situ fracturing of quartz (Fig. 9a,b). This may be the evidence of super saturated fluids that could form in early stages of the experiment when a metastable solid phase is present, e.g. albite glass, REE-rich allanite. In fact, in the case of allanite, the overgrowth rim around starting allanite seeds is represented by relatively REE-depleted allanite at 800 °C, which would explain the lower LREE concentrations in the equilibrium fluid after sufficient time has elapsed for the formation of the REE-poorer allanite overgrowth. However, the same effect related to super saturation is not observed for LREE at 700 °C where a zoisite rim formed around original allanite. A plausible reason for this is a larger deviation from equilibrium of the starting allanite at 700 ^{o}C (i.e. the thermodynamically stable phase is zoisite), which may induce a faster dissolution-precipitation process, before the healing of the fractures in quartz is completed.

Implications and concluding remarks

A new approach has been developed to investigate complex aqueous fluid – rock equilibria at high *P* conditions relevant for slab dehydration processes (~ 2.5 – 3.0 GPa, 88 - 105 km depth). The proposed experimental strategy allows sampling aqueous fluids, previously equilibrated with

444 a quartz-saturated solid mineral assemblage, at high $P - T$ conditions in the form of synthetic
445 fluid inclusions in quartz. To provide sufficient time for the achievement of fluid – rock
446 equilibrium, the quartz crystal is fractured in-situ during the experiment by crossing the quartz -
447 coesite transition boundary. Although this approach restricts the investigated P - T conditions to
448 near the quartz - coesite phase boundary, it extends reliability of the synthetic fluid inclusion
449 technique to conditions relevant to slab dehydration beyond crustal depths. The results on
450 selected major/trace element (Ti, Na, Mg, REE, Zr, Sr, Ba and Nb) solubility reported in this
451 study demonstrate the feasibility of the method, as well as the importance of in-situ fracturing vs.
452 ex-situ/pre-fracturing of quartz to sample true equilibrium fluids.

453 Overall, the proposed approach compliments the existing methodologies and provides
454 further progress in investigating the chemistry of aqueous fluids at sub-arc conditions. The
455 application of this technique has the potential to improve our understanding of the role of
456 aqueous fluids in mass transfer and recycling processes in subduction-zones.

457

458 **Acknowledgments**

459 We would like to thank Peter Tropper, Codi Lazar and an anonymous reviewer for their
460 constructive reviews, which were helpful to improve the quality of this manuscript. Furthermore,
461 we are very grateful to Dionysis Foustoukos for the editorial handling of the manuscript and for
462 his constructive comments. Alexandra Tsay also acknowledges the SNSF early postdoc Mobility
463 fellowship (No. P2EZP2_155583).

464

465

References cited

Aerts, M., Hack, A.C., Reusser, E., and Ulmer, P. (2010) Assessment of the diamond-trap method for studying high-pressure fluids and melts and an improved freezing stage design for laser ablation ICP-MS analysis. American Mineralogist, 95(10), 1523-1526.

Bali, E., Audetat, A., and Keppler, H. (2011) The mobility of U and Th in subduction zone fluids: an indicator of oxygen fugacity and fluid salinity. Contributions to Mineralogy and Petrology, 161(4), 597-613.

Bali, E., Keppler, H., and Audetat, A. (2012) The mobility of W and Mo in subduction zone fluids and the Mo-W-Th-U systematics of island arc magmas. Earth and Planetary Science Letters, 351, 195-207.

Bali, E., Audetat, A., and Keppler, H. (2013) Water and hydrogen are immiscible in Earth's mantle. Nature, 495, 220-222.

Basset, W.A., Shen, A.H., Bucknum, M., and Chou, I.-M. (1993) A new diamond anvil cell for hydrothermal studies to 10 GPa and 190 °C to 1100 °C. Review of Scientific Instruments, 64, 2340-2345.

Basset, W.A., Anderson, A.J., Mayanovic, R.A., and I-.M. Chou (2000) Modified hydrothermal diamond anvil cells for XAFS analysis of elements with low energy absorption edges in aqueous solutions at sub- and supercritical conditions. Zeitschrift fur Kristallographie, 215, 711-717.

Bodnar, R.J., and Sterner, S.M. (1987) Synthetic fluid inclusions. In: Ulmer, G.C., Barnes, H.L. (Ed.), Hydrothermal Experimental Technique Wiley-Interscience, New York, 423-457.

Bohlen, S.R., Essene, E.J., and Boettcher, A.L. (1980) Reinvestigation and application of olivine-quatyz-orthopyroxene barometry. Earth and Planetary Science Letters, 47(1), 1-10.

Bose, K., and Ganguly, J. (1995) Quartz-coesite transition revisited - reversed experimental determination at 500 - 1200 degrees C and retrieved thermochemical properties. American Mineralogist, 80(3-4), 231-238.

Brenan, J.M., Shaw, H.F., Ryerson, F.J., and Phinney, D.L. (1995a) Experimental determination of trace element partitioning between pargasite and a synthetic andesitic melt. Earth and Planetary Science Letters, 135(1-4), 1-11.

Bureau, H., Foy, E., Raepsaet, C., Somogyi, A., Munsch, P., Simon, G., and Kubsky, S. (2010) Bromine cycle in subduction zones through in-situ Br monitoring in diamond anvil cell. Geochimica et Cosmochimica Acta, 74, 3839-3850.

Caciagli, N.C., and Manning, C.E. (2003) The solubility of calcite in water at 6-16 kbar and 500-800 degrees C. Contributions to Mineralogy and Petrology, 146(3), 275-285.

Churakov, S.V., and Gottschalk, M., (2003a) Perturbation theory based equation of state for polar molecular fluids: I. Pure fluids. Geochimica et Cosmochimica Acta, 67, 2397-2414.

Fujimaki, H. (1986) Partition coefficients of Hf, Zr and REE between zircon, apatite and liquid. Contributions to Mineralogy and Petrology, 94(1), 42-45.

Guillong, M., and Heinrich, C.A. (2007) Sensitivity enhancement in laser ablation ICP-MS using small amounts of hydrogen in the carrier gas. Journal of Analytical Atomic Spectrometry, 22(12), 1488-1494.

Gunther, D., and Heinrich, C.A. (1999) Comparison of the ablation behaviour of 266 nm Nd : YAG and 193 nm ArF excimer lasers for LA-ICP-MS analysis. Journal of Analytical Atomic Spectrometry, 14(9), 1369-1374.

Heinrich, C.A., Pettke, T., Halter, W.E., Aigner-Torres, M., Audetat, A., Gunther, D., Hattendorf, B., Bleiner, D., Guillong, M., and Horn, I. (2003) Quantitative multi-element analysis of

512 minerals, fluid and melt inclusions by laser-ablation inductively-coupled-plasma mass-
513 spectrometry. Geochimica Et Cosmochimica Acta, 67(18), 3473-3497.
514 Hermann, J., and Rubatto, D. (2009) Accessory phase control on the trace element signature of
515 sediment melts in subduction zones. Chemical Geology, 265(3-4), 512-526.
516 Hermann, J., and Spandler, C.J. (2008) Sediment melts at sub-arc depths: An experimental study.
517 Journal of Petrology, 49(4), 717-740.
518 Kessel, R., Schmidt, M.W., Ulmer, P., and Pettke, T. (2005a) Trace element signature of
519 subduction-zone fluids, melts and supercritical liquids at 120-180 km depth. Nature,
520 437(7059), 724-727.
521 Kessel, R., Ulmer, P., Pettke, T., Schmidt, M.W., and Thompson, A.B. (2004) A novel approach
522 to determine high-pressure high-temperature fluid and melt compositions using diamond-
523 trap experiments. American Mineralogist, 89(7), 1078-1086.
524 Kessel, R., Ulmer, P., Pettke, T., Schmidt, M.W., and Thompson, A.B. (2005b) The water-basalt
525 system at 4 to 6 GPa: Phase relations and second critical endpoint in a K-free eclogite at
526 700 to 1400 degrees C. Earth and Planetary Science Letters, 237(3-4), 873-892.
527 Klemme, S., Blundy, J.D., and Wood, B.J. (2002) Experimental constraints on major and trace
528 element partitioning during partial melting of eclogite. Ceochimica Et Cosmochimica
529 Acta, 66(17), 3109-3123.
530 Klemme, S., Prowatke, S., Hametner, K., and Gunther, D. (2005) Partitionng of trace elements
531 between rutile and silicate melts: Implication for subduction zones. Geochimica Et
532 Cosmochimica Acta, 69(9), 2361-2371.
533 Klimm, K., Blundy, J.D., and Green, T.H. (2008) Trace element partitioning and accessory phase
534 saturation during H2O-saturated melting of basalt with implications for subduction zone
535 chemical fluxes. Journal of Petrology, 49(3), 523-553.

536 Kushiro, I., and Hirose, K. (1992) Experimental determination of composition of melt formed by
537 equilibrium partial melting of peridotite at high pressures using aggregates of diamond
538 grains. Proceedings of the Japan Academy series B-physical and biological sciences, 68,
539 63– 68.
540 Louvel, M., Sanchez-Valle, C., Malfait, W.J., Tesmale, D., and Hazemann, J.-L. (2013) Zr
541 complexation in high pressure fluids and silicate melts and implication for the
542 mobilization of HFSE in subduction zones. Geochimica Et Cosmochimica Acta, 104,
543 281-299.
544 Manning, C.E. (1994) The solubility of quartz in H2O in the lower crust and upper-mantle.
545 Geochimica Et Cosmochimica Acta, 58(22), 4831-4839.
546 Manning, C.E., 2004. The chemistry of subduction-zone fluids. Earth and Planetary Science
547 Letters, 223(1-2), 1-16.
548 Manning, C.E., Wilke M., Schmidt C., and Cauzid J. (2008) Rutile solubility in albite-H_2O and
549 $Na_2Si_3O_7$-H_2O at high temperatures and pressures by in-situ synchrotron radiation micro-
550 XRF. Earth and Planetary Science Letters, 272, 730-737.
551 Mayanovic, R.A., Jayanetti, S., Anderson, A.J., Bassett, W.A., and Chou, I.-M. (2002) The
552 structure of Yb3+ aquo ion and chloro complexes in aqueous solutions at up to 500°C and
553 270 MPa. Journal of Physical Chemistry A, 106, 6591-6599.
554 Poli, S., and Schmidt, M.W. (2002) Petrology of subducted slabs. Annual Review of Earth and
555 Planetary Sciences, 30, 207-235.
556 Prowatke, S., and Klemme, S. (2006) Trace element partitioning between apatite and silicate
557 melts. Geochimica Et Cosmochimica Acta, 70(17), 4513-4527.

558 Ryabchikov, I.D., and Boettcher, A.L. (1980) Experimental-evidence at high-pressure for
559 potassic metasomatism in the mantle of the earth. American Mineralogist, 65(9-10), 915-
560 919.
561 Sanchez-Valle, C., Martinez, I., Daniel, I., Philippot, P., Bonic, S., and Simionovici, A. (2003)
562 Dissolution of strontianite at high P-T conditions: An in-situ synchrotron X-ray
563 fluorescence study. American Mineralogist, 88, 978-985.
564 Sanchez-Valle, C. (2013) Structure and thermodynamics of subduction zone fluids from
565 spectroscopic studies. Reviews in Mineralogy and Geochemistry, 76, 1, 265-309.
566 Scambelluri, M., and Philippot, P. (2001) Deep fluids in subduction zones. Lithos, 55(1-4), 213-
567 227.
568 Schmidt, M.W., and Ulmer, P. (2004) A rocking multianvil: Elimination of chemical segregation
569 in fluid-saturated high-pressure experiments. Geochimica Et Cosmochimica Acta, 68(8),
570 1889-1899.
571 Skora, S., and Blundy, J. (2012) Monazite solubility in hydrous silicic melts at high pressure
572 conditions relevant to subduction zone metamorphism. Earth and Planetary Science
573 Letters, 321, 104-114.
574 Spandler, C., Mavrogenes, J., and Hermann, J. (2007) Experimental constraints on element
575 mobility from subducted sediments using high-P synthetic fluid/melt inclusions. Chemical
576 Geology, 239(3-4), 228-249.
577 Spandler, C., and Pirard, C. (2013) Element recycling from subducting slabs to arc crust: A
578 review. Lithos, 170, 208-223.
579 Stalder, R., Foley, S.F., Brey, G.P., and Horn, I. (1998) Mineral aqueous fluid partitioning of
580 trace elements at 900-1200 degrees C and 3.0-5.7 GPa: New experimental data for garnet,

clinopyroxene, and rutile, and implications for mantle metasomatism. Geochimica Et Cosmochimica Acta, 62(10), 1781-1801.

Sterner, S.M., and Bodnar, R.J. (1984) Synthetic fluid inclusions in natural quartz. 1. Compositional types synthesized and applications to experimental geochemistry. Geochimica Et Cosmochimica Acta, 48(12), 2659-2668.

Thomas, J.B., Bodnar, R.J., Shimizu, N., and Sinha, A.K. (2002) Determination of zircon/melt trace element partition coefficients from SIMS analysis of melt inclusions in zircon. Ceochimica et Cocmochimica Acta, 66(16), 2887-2901.

Tropper, P., and Manning, C.E. (2005) Very low solubility of rutile in H2O at high pressure and temperature, and its implications for Ti mobility in subduction zones. American Mineralogist, 90(2-3), 502-505.

Tsay, A., Zajacz, Z., and Sanchez-Valle, C. (2014) Efficient mobilization and fractionation of rare-earth elements by aqueous fluids upon slab dehydration. Earth and Planetary Science Letters, 398, 101-112.

Ulmer, P. (2001) Partial melting in the mantle wedge - the role of H(2)O in the genesis of mantle-derived 'arc-related' magmas. Physics of the Earth and Planetary Interiors, 127(1-4), 215-232.

Wilke, M., Schmidt, C., Dubrail, J., Appel, K., Borchert, M., Kvashina, K., and Manning, C.E. (2012) Ziron solubility and zirconium complexation in H2O+Na2O+SiO2±Al2O3 fluids at high pressure and temperature. Earth and Planetary Science Letters, 349-350, 15-25.

Zajacz, Z., Seo, J.H., Candela, P.A., Piccoli, P.M., Heinrich, C.A., and Guillong, M. (2010) Alkali metals control the release of gold from volatile-rich magmas. Earth and Planetary Science Letters, 297(1-2), 50-56.

605 **List of figure captions:**

606 **Fig. 1.** Phase diagram for the silica system; red symbols indicate the equilibration conditions of
607 the experiment and arrows with numbers follow the *P* – *T* path of the experimental procedure: (1)
608 the solid and fluid phases are equilibrated at the nominal *P* and *T*; (2) the sample is compressed
609 across the quartz – coesite transition boundary; (3) the sample is quenched down to ~ 300 °C to
610 induce a sudden decompression; (4) the sample is reheated and compressed back to the nominal *P*
611 and *T* to form the synthetic fluid inclusions (SFI).

612 **Fig. 2.** Sketches of different piston cylinder assemblies employed in this study: (**a**) – MgO or BN
613 sleeve around the capsule with pyrex and talc surrounding the graphite furnace; (**b**) – similar to
614 assembly type (**a**) but with pyrex sleeve surrounding the capsule; (**c**) – BN tube around the
615 capsule with a salt (NaCl) cell surrounding the graphite furnace; MgO served as thermocouple
616 sleeve in assembly type (**a**) but was replaced by Al_2O_3 in (**b**) and (**c**).

617 **Fig. 3.** Sketches of the capsule arrangements. Au was used as a capsule material; the external
618 capsule was loaded with an pristine quartz core of cylindrical shape, an internal capsule with the
619 starting material and an aqueous fluid with/without albite glass: (**a**) – with infiltrating layers of
620 zirconia spheres or zircon fragments on the top and the bottom of the internal capsule; (**b**) – with
621 large fragments (> 100 μm) of accessory phases and garnet in the external capsule; (**c**) – with two
622 kinds of quartz crystals, pre-fractured before the experiment and a pristine one that will be
623 fractured in-situ.

624 **Fig. 4.** Backscattered electron images of run products, showing: (**a**) - a layer of ZrO_2 and (**b**) -
625 zircon fragments in contact with mineral assemblage on the bottom of the internal capsules; (**c** -
626 **d**) - phase relations and reaction rims grown around mineral phases in # 63 at 700 °C and 2.5 GPa
627 (**c**) and # 62 at 800 °C and 2.6 GPa (**d**).

628 **Fig. 5.** Microphotographs of SFI in quartz: (**a**) – channels of primary FI fluid inclusions in the
629 overgrowth zone of quartz crystal from # 54; (**b – c**) – secondary FI formed upon in-situ
630 fracturing of quartz from # 58 (**b**) and 63 (**c**); (**d**) – secondary FI formed in the pre-fractured
631 quartz crystal from # 69.

632

Fig. 6. (**a**) Rare-earth element (REE) concentrations in the fluid at 800 °C from experiments with different solid/fluid (s/f) ratios and Na content added in the form of albite glass; (**b**) comparison between the REE pattern of allanite and the patterns from experiments with different Na content (i.e. added albite glass). Error bars represent 1 σ uncertainties calculated as a standard deviation; arrows indicate that the plotted concentration corresponds to the detection limit.

Fig. 7. Element concentrations in secondary fluid inclusions at 700 °C formed by in-situ (# 63) and ex-situ (# 69, 95) fracturing of quartz, as well as in primary fluid inclusions (# 69). With the exception of Na, the elemental concentrations are consistently higher in inclusions formed by in-situ fracturing than in those formed by ex-situ fracturing of quartz. A clear correlation between different groups of inclusions is observed for Sr, Nb and Ti contents, showing three groups of compositions where the composition of primary inclusions is intermediate between the secondary inclusions formed by in-situ and ex-situ fracturing of quartz.

Fig. 8. Trace element concentrations in secondary fluid inclusions at 800 °C formed by in-situ (# 62) and ex-situ (# 93) fracturing of quartz. The concentrations for all elements are significantly higher in the in-situ fractured experiment compared to the ex-situ fractured one.

Fig. 9. Major and REE concentrations in secondary fluid inclusions at 800 °C formed by in-situ (# 62) and ex-situ (# 93) fracturing of quartz. All major elements, except Na, show higher concentrations in in-situ fractured experiment (**a**), whereas light rare-earth elements (LREE) show the opposite (**b**). A possible explanation for higher LREE concentrations in ex-situ fractured experiment is most likely the fact that the fluid sampled in early stages of the experiment is interacting with an initially more REE-rich allanite (see details in section "Comparison between ex-situ and in-situ fracturing of quartz").

660 **Footnotes:**

661 * Corresponding author. Present address: Department of Earth Sciences, University of Toronto,
662 22 Russell St., M5S 3B1, Toronto, Canada. Email: a.tsay@utoronto.ca

663 **Table 1**. Notes: Mineral abbreviations: Px – pyroxene, Grt – garnet, Aln – allanite, Ky – kyanite,
664 Zrn – zircon, Rut – rutile. Glass II corresponds to bulk composition of the second starting
665 material, i.e. a mechanical mixture of mineral phases. [a] Trace element concentrations shown in
666 wt.% of element oxides. Major elements, REE in Aln and Zr in Zrn were analyzed by electron
667 microprobe; trace elements in all other phases were analyzed by LA-ICPMS; n - corresponds to
668 number of measurements; f.u. – corresponds to mineral formulae units normalized for a fixed
669 number of cations (i.e. 4 for Px and 8 for Grt and Aln); all Fe is considered as Fe^{2+}; 1σ
670 uncertainties are shown in parentheses on the last significant digit calculated as a standard
671 deviation; n.a. not analyzed; <lod below limit of detection.
672 **Table 2**. Notes: a The pressure in parentheses corresponds to the compression step during the
673 experiment to cross the quartz – coesite transition boundary (Fig. 1). b The two durations shown
674 for a single experiment indicate the run duration before and after the quartz – coesite transition,
675 respectively; in experiments with only one run duration, the quartz - coesite transition method
676 was not applied (# 49) or the quartz crystal was pre-fractured before the experiment (# 69). c
677 Starting material: I, natural eclogite; II, ~ 67 wt.% omphacite, ~ 19 wt.% garnet, ~ 9 wt.%
678 kyanite, ~ 3 wt.% allanite, ~ 1 wt.% and ~ 1 wt.% rutile; XAlbite – mol fraction of albite glass
679 added to the charge. d Type of capsule arrangement (Fig.3). “Fluid” and “Fractures” indicate the
680 presence or absence of fluid and fractures (in quartz) after the experiment, respectively.

681

This is a preprint, the final version is subject to change, of the American Mineralogist (MSA)
Cite as Authors (Year) Title. American Mineralogist, in press.
(DOI will not work until issue is live.) DOI: http://dx.doi.org/10.2138/am-2016-5621

Table 1. Compositions of the mineral phases and the bulk starting material.

	Px		Grt		Aln		Ky	Zrn	Rut	Glass II
wt. %	*n = 7*	*f.u.*	*n = 15*	*f.u.*	*n = 14*	*f.u.*	*n = 5*	*n = 5*	*n = 5*	*n = 7*
SiO_2	55.1(1)	*1.98*	40.3(2)	*3.01*	33.3(9)	*3.04*	36.9(1)	33.4(2)	0.01(1)	48.6(4)
TiO_2	0.11(2)	*0.00*	0.05(1)	*0.00*	0.3(1)	*0.02*	<lod	0.01(1)	97.6(4)	1.09(5)
Al_2O_3	6.7(2)	*0.28*	22.4(1)	*1.97*	18.8(7)	*2.03*	62.9(1)	<lod	0.06(2)	15.7(2)
FeO	4.5(2)	*0.13*	19.8(9)	*1.23*	5.1(7)	*0.39*	0.11(3)	0.01(1)	1.10(3)	7.23(5)
MgO	11.5(2)	*0.61*	9.7(8)	*1.08*	4.3(6)	*0.58*	<lod	0.01(1)	0.01(1)	9.62(7)
MnO	0.02(1)	*0.00*	0.47(1)	*0.03*	n.a.	*n.a.*	n.a.	n.a.	n.a.	0.11(2)
CaO	18.3(2)	*0.70*	8.4(5)	*0.67*	11.0(6)	*1.08*	<lod	0.01(1)	0.01(1)	12.6(1)
Na_2O	4.05(14)	*0.28*	0.03(2)	*0.00*	n.a.	*n.a.*	n.a.	n.a.	n.a.	2.8(1)
K_2O	0.01(1)	*0.00*	<lod	*0.00*	n.a.	*n.a.*	n.a.	n.a.	n.a.	0.02(1)
Total	100.2(3)		101.1(3)		99.1(2.6)		99.9(2)	98.5(5)	98.8(3)	97.7(6)
ppm	*n = 6*		*n = 4*		*n = 4*		n = 3	*n = 3*	*n = 3*	*n = 4*
Sr	61(19)		<0.07		45(3)		<0.03	0.14(2)	0.58(5)	262(1)
Ba	0.76(17)		<0.34		n.a.		<0.17	0.08	0.14	18.1(8)
Nb	0.03		<0.07		n.a.		<0.03	5.0(1.1)	3622(254)	32.1(4)
Zr	1.3(3)		1.9(5)		n.a.		<0.07	65.1(4) [a]	306(5)	4128(75)
La	<0.03		<0.05		5.7(5) [a]	*0.19*	0.02	0.04(2)	<0.02	1241(7)
Ce	0.10(3)		<0.06		11.85(54) [a]	*0.4*	<0.02	14(5)	0.10(8)	2726(52)
Pr	0.04(2)		<0.02		1.68(13) [a]	*0.06*	0.01	0.15(9)	0.02	336(3)
Nd	0.39(3)		<0.31		5.96(53) [a]	*0.19*	<0.16	2.3(1.2)	<0.09	1292(6)
Sm	0.4(1)		<0.41		0.87(22) [a]	*0.03*	<0.16	3.1(1.4)	<0.08	230(2)
Eu	0.19(5)		<0.08		604(110)		<0.05	2.1(1.1)	<0.03	17.6(1)
Gd	0.6(2)		<0.44		0.31(16) [a]	*0.01*	<0.2	11.1(5.8)	<0.14	105(1)
Dy	0.32(9)		0.97(36)		525(83)		<0.1	28(14)	<0.07	19.7(1)
Yb	0.15		2.6(2.0)		56(5)		<0.18	57(24)	<0.15	4.1(1)
Y	0.7(2)		10.8(3.6)		1211(92)		<0.03	261(127)	0.073(2)	51.2(6)
Th	<0.04		<0.06		45 (14)		<0.04	98(71)	0.04	0.91(2)
U	0.02		<0.05		n.a.		<0.03	88 (49)	46.3(1.7)	0.66(2)

Notes: Mineral abbreviations: Px – pyroxene, Grt – garnet, Aln – allanite, Ky – kyanite, Zrn – zircon, Rut – rutile. Glass II corresponds to bulk composition of the second starting material, i.e. a mechanical mixture of mineral phases (section 2.2). [a] Trace element concentrations shown in wt.% of element oxides. Major elements, REE in Aln and Zr in Zrn were analyzed by electron microprobe; trace elements in all other phases were analyzed by LA-ICPMS; n - corresponds to number of measurements; f.u. – corresponds to mineral formulae units normalized for a fixed number of cations (i.e. 4 for Px and 8 for Grt and Aln), all Fe is considered as Fe^{2+}; 1σ uncertainties are shown in parentheses on the last significant digit calculated as a standard deviation; n.a. - not analyzed; <lod - below limit of detection.

Table 2. Experimental details.

Exp No.	T (°C)	P (GPa)	Assembly type	P (friction) (%)	Duration (hours)[b]	Starting Material[c]	X_{Albite}	Solid/fluid (mass ratio)	Infiltrating medium	Fluid	Fractures
# 48	800	2.6-(3.3)[a]	BN-Pyrex-Talc	-10	45+24	I	-	1	ZrO_2 (a)[d]	no	no
# 49	800	2.6	BN-Pyrex-Talc	-10	72	I	-	1	ZrO_2 (a)	no	no
# 50	800	2.6-(3.3)	MgO-Pyrex-Talc	-10	77+48	I	-	1	ZrO_2 (a)	yes	yes
# 51	800	2.6-(3.3)	MgO-Pyrex-Talc	-10	120+48	I	-	1	ZrO_2 (a)	yes	no
# 52	800	2.6-(3.3)	Pyrex-Pyrex-Talc	-10	68+27	II	-	1.7	ZrO_2 (a)	yes	yes
# 54	800	2.6-(3.3)	Pyrex-Pyrex-Talc	-10	96+48	II	0.04	2	ZrO_2 (a)	yes	no
# 58	800	2.6-(3.4)	BN-NaCl	-5	96+51	II	0.04	1.7	- (b)	yes	yes
# 62	800	2.6-(3.4)	BN-NaCl	-5	119+47	II	0.02	1.7	- (b)	yes	yes
# 93	800	2.6	BN-NaCl	-5	48	II	0.02	1.7	- (c)	yes	yes
# 56	700	2.5-(3.3)	BN-NaCl	-5	123+48	II	0.02	1.7	Zrn (a)	yes	yes
# 63	711	2.5-(3.3)	BN-NaCl	-5	141+74	II	0.01	1.7	- (b)	yes	yes
# 69	700	2.5	BN-NaCl	-5	117	II	0.01	1.7	- (c)	yes	yes
#95	700	2.5	BN-NaCl	-5	44	II	0.01	1.7	- (c)	yes	yes

Notes: [a] The pressure in parentheses corresponds to the compression step during the experiment to cross the quartz – coesite transition boundary (Fig. 1). [b] The two durations shown for a single experiment indicate the run duration before and after the quartz – coesite transition, respectively; in experiments with only one run duration, the quartz - coesite transition method was not applied (# 49) or the quartz crystal was pre-fractured before the experiment (# 69). [c] Starting material: I, natural eclogite; II, ~ 67 wt.% omphacite, ~ 19 wt.% garnet, ~ 9 wt.% kyanite, ~ 3 wt.% allanite, ~ 1 wt.% and ~ 1 wt.% rutile; X_{Albite} – mol fraction of albite glass added to the charge. [d] Type of capsule arrangement (Fig.3). "Fluid" and "Fractures" indicate the presence or absence of fluid and fractures (in quartz) after the experiment, respectively.

This is a preprint, the final version is subject to change, of the American Mineralogist (MSA)
Cite as Authors (Year) Title. American Mineralogist, in press.
(DOI will not work until issue is live.) DOI: http://dx.doi.org/10.2138/am-2016-5621

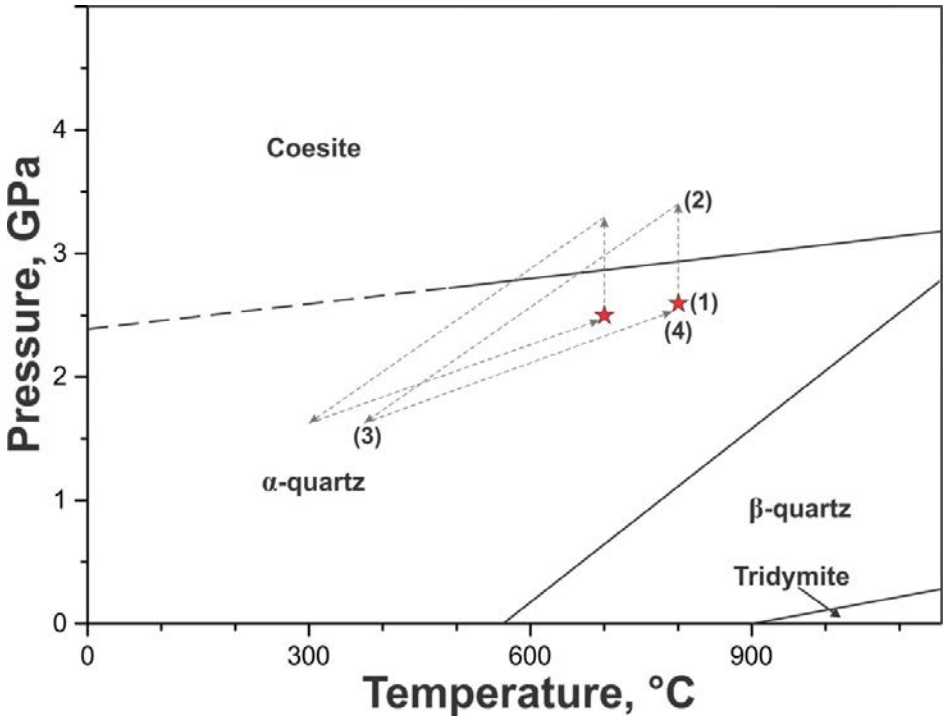

Figure 1

This is a preprint, the final version is subject to change, of the American Mineralogist (MSA)
Cite as Authors (Year) Title. American Mineralogist, in press.
(DOI will not work until issue is live.) DOI: http://dx.doi.org/10.2138/am-2016-5621

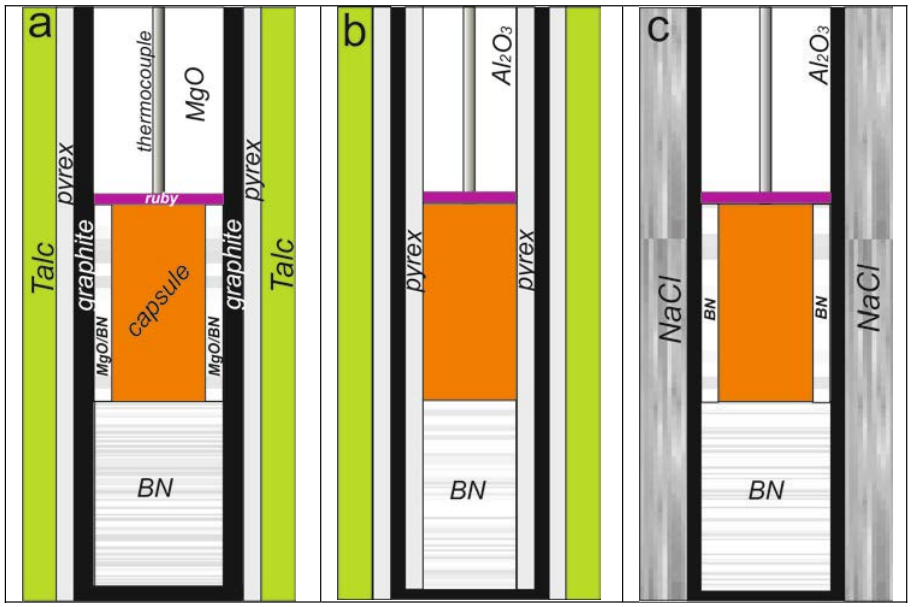

Figure 2

This is a preprint, the final version is subject to change, of the American Mineralogist (MSA)
Cite as Authors (Year) Title. American Mineralogist, in press.
(DOI will not work until issue is live.) DOI: http://dx.doi.org/10.2138/am-2016-5621

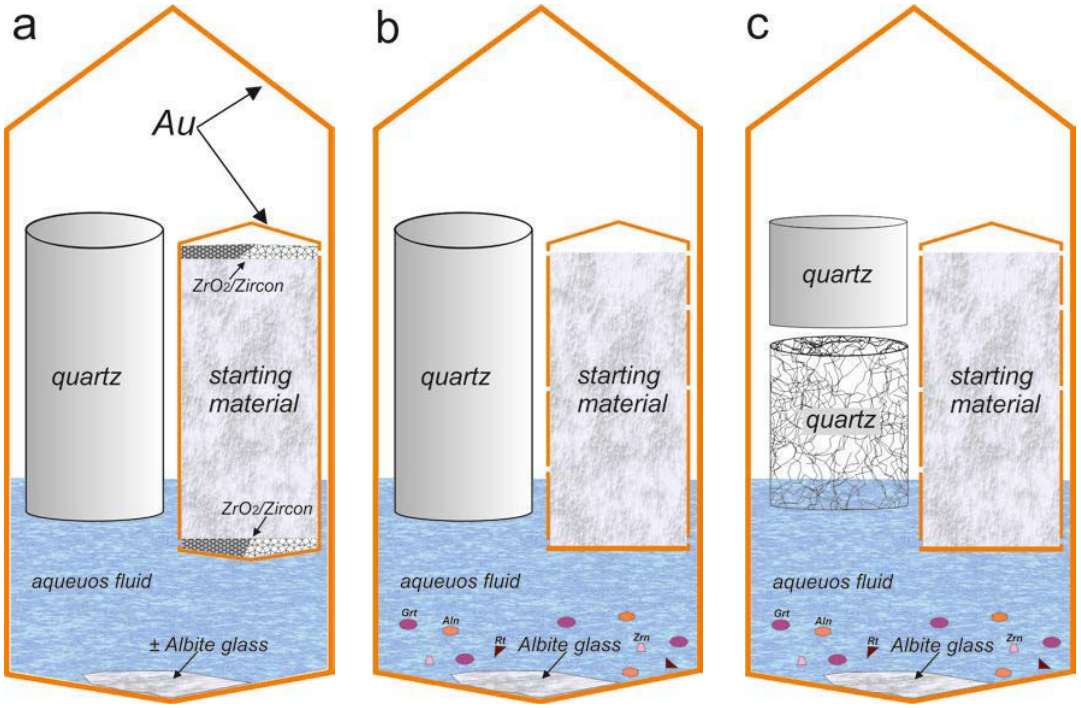

Figure 3

This is a preprint, the final version is subject to change, of the American Mineralogist (MSA)
Cite as Authors (Year) Title. American Mineralogist, in press.
(DOI will not work until issue is live.) DOI: http://dx.doi.org/10.2138/am-2016-5621

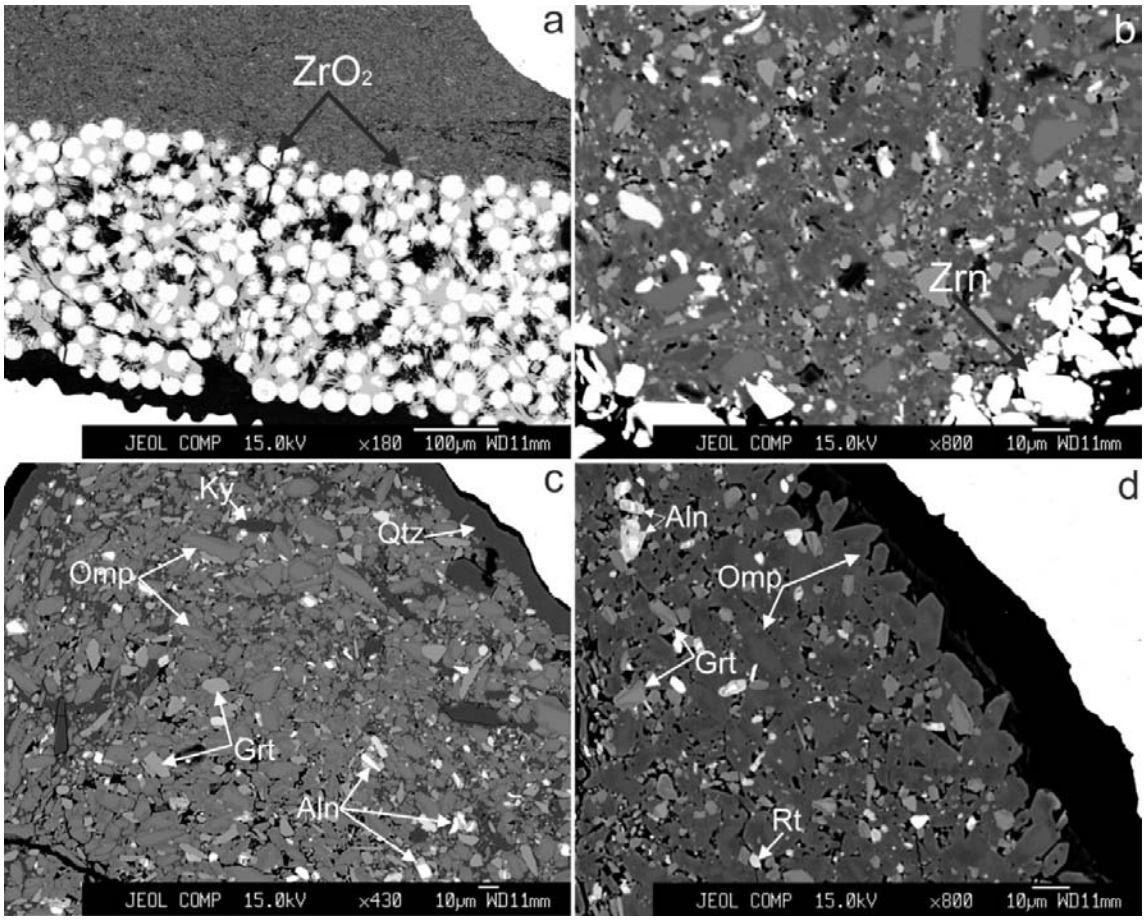

Figure 4

This is a preprint, the final version is subject to change, of the American Mineralogist (MSA)
Cite as Authors (Year) Title. American Mineralogist, in press.
(DOI will not work until issue is live.) DOI: http://dx.doi.org/10.2138/am-2016-5621

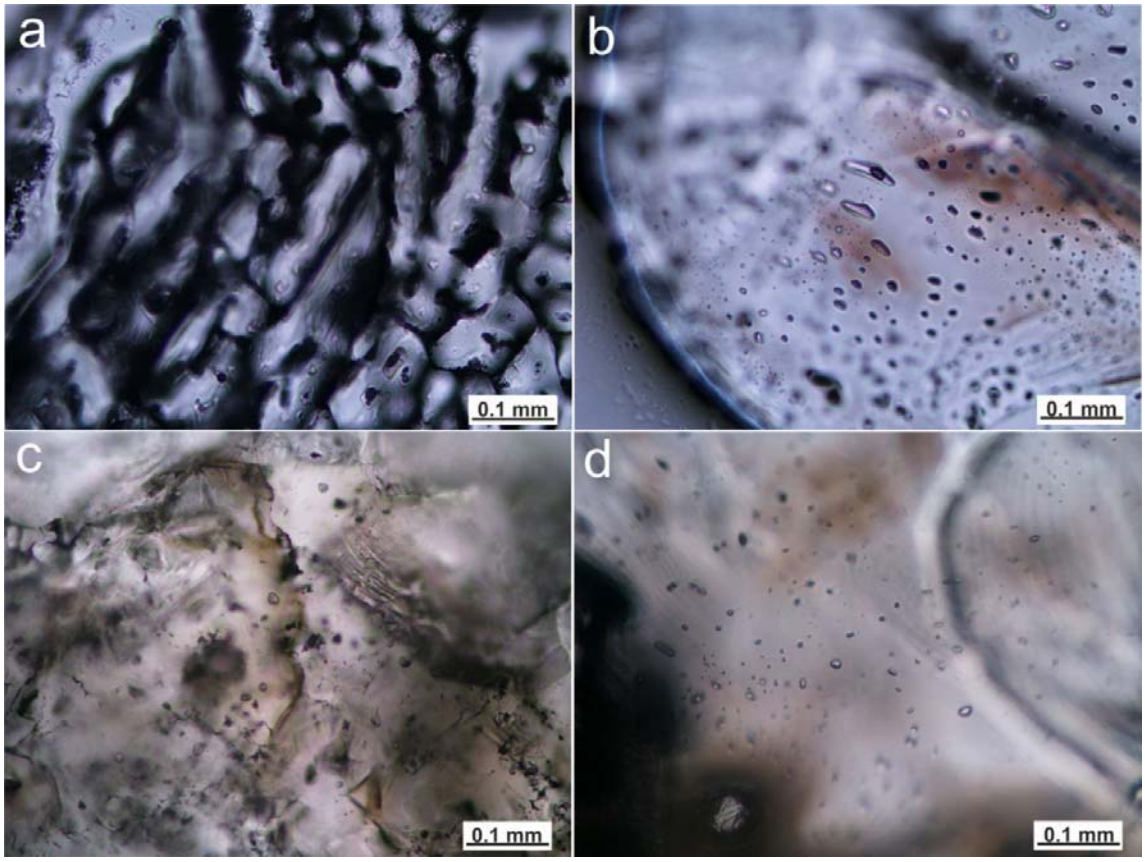

Figure 5

This is a preprint, the final version is subject to change, of the American Mineralogist (MSA)
Cite as Authors (Year) Title. American Mineralogist, in press.
(DOI will not work until issue is live.) DOI: http://dx.doi.org/10.2138/am-2016-5621

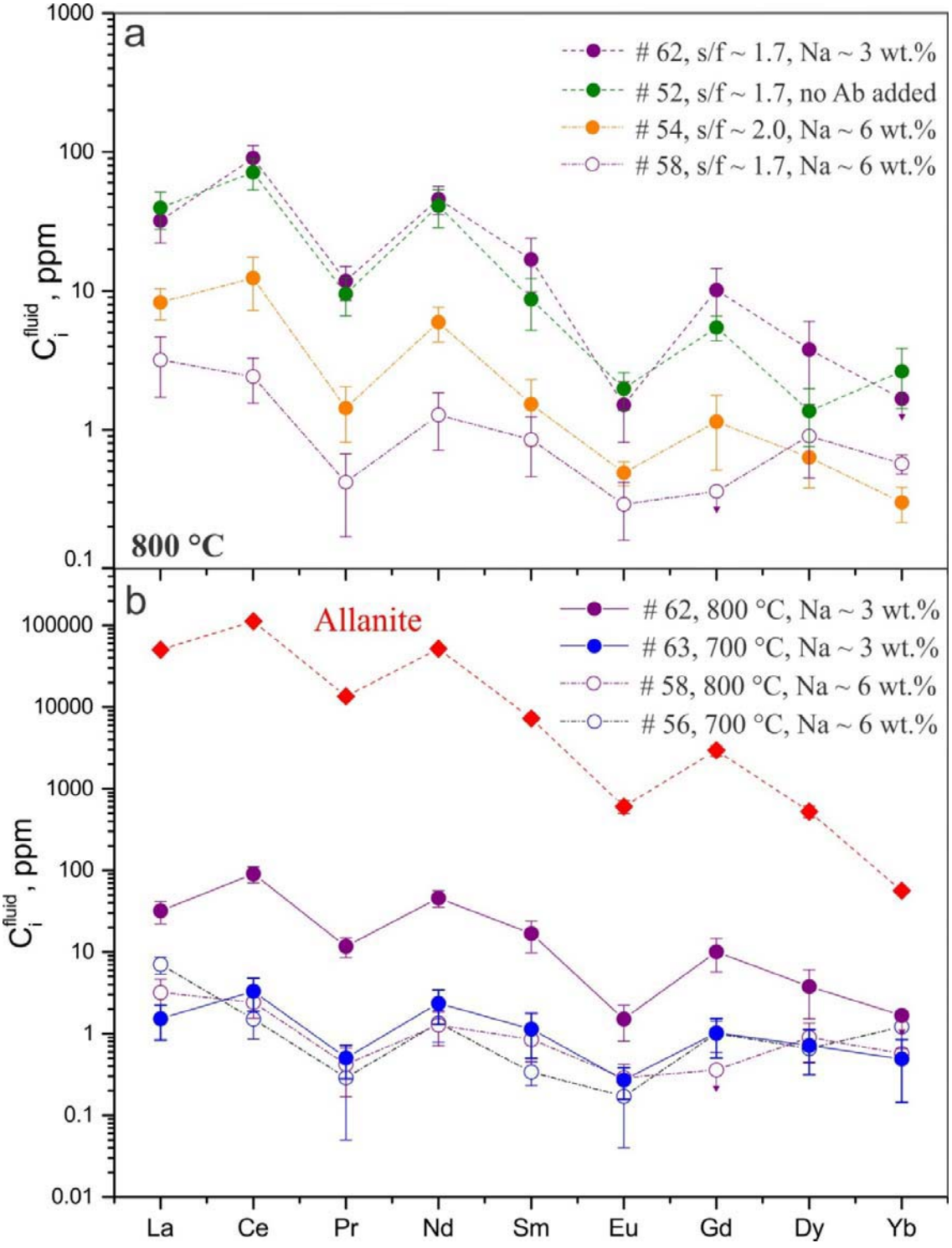

Figure 6

This is a preprint, the final version is subject to change, of the American Mineralogist (MSA)
Cite as Authors (Year) Title. American Mineralogist, in press.
(DOI will not work until issue is live.) DOI: http://dx.doi.org/10.2138/am-2016-5621

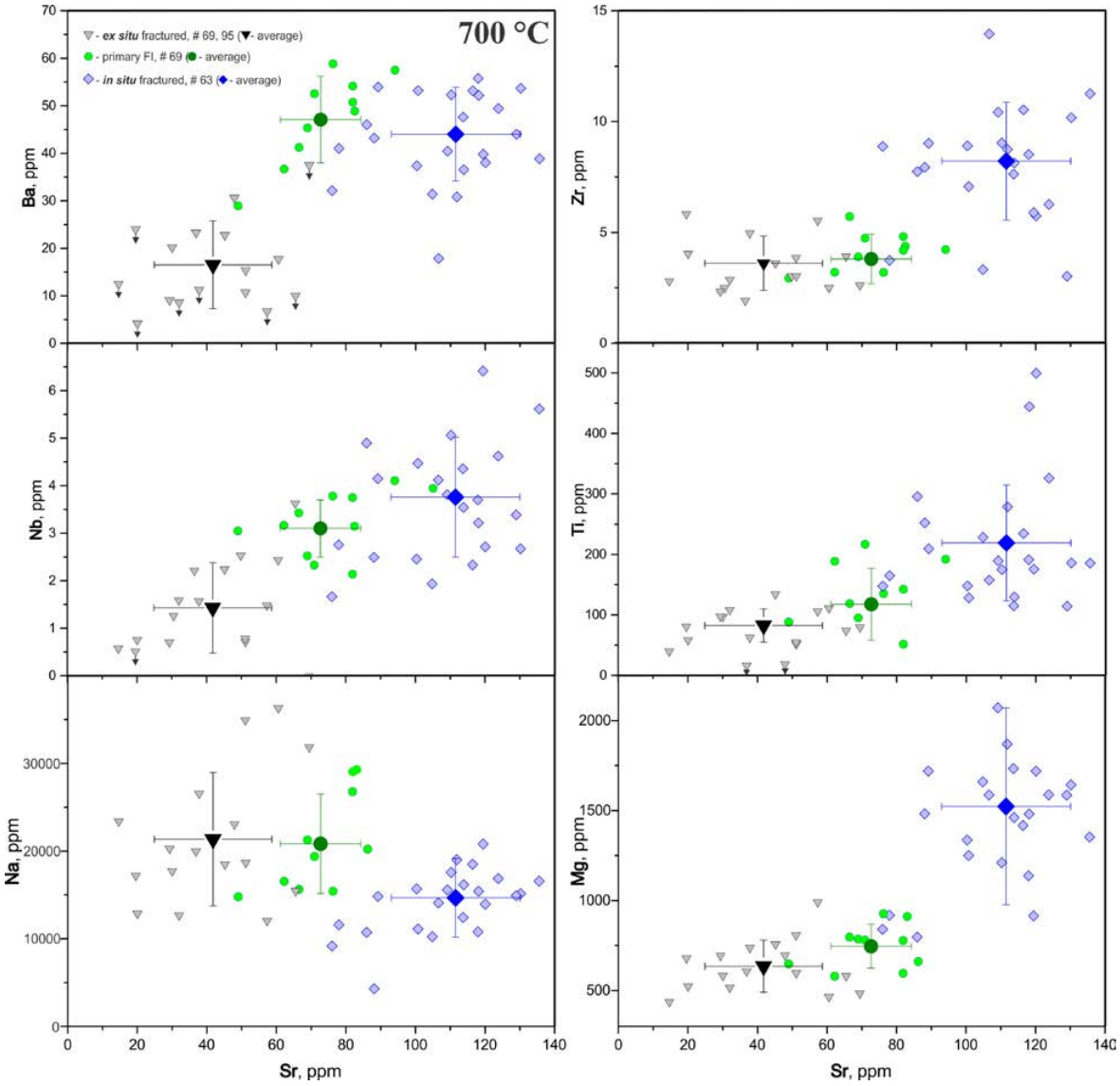

Figure 7

This is a preprint, the final version is subject to change, of the American Mineralogist (MSA)
Cite as Authors (Year) Title. American Mineralogist, in press.
(DOI will not work until issue is live.) DOI: http://dx.doi.org/10.2138/am-2016-5621

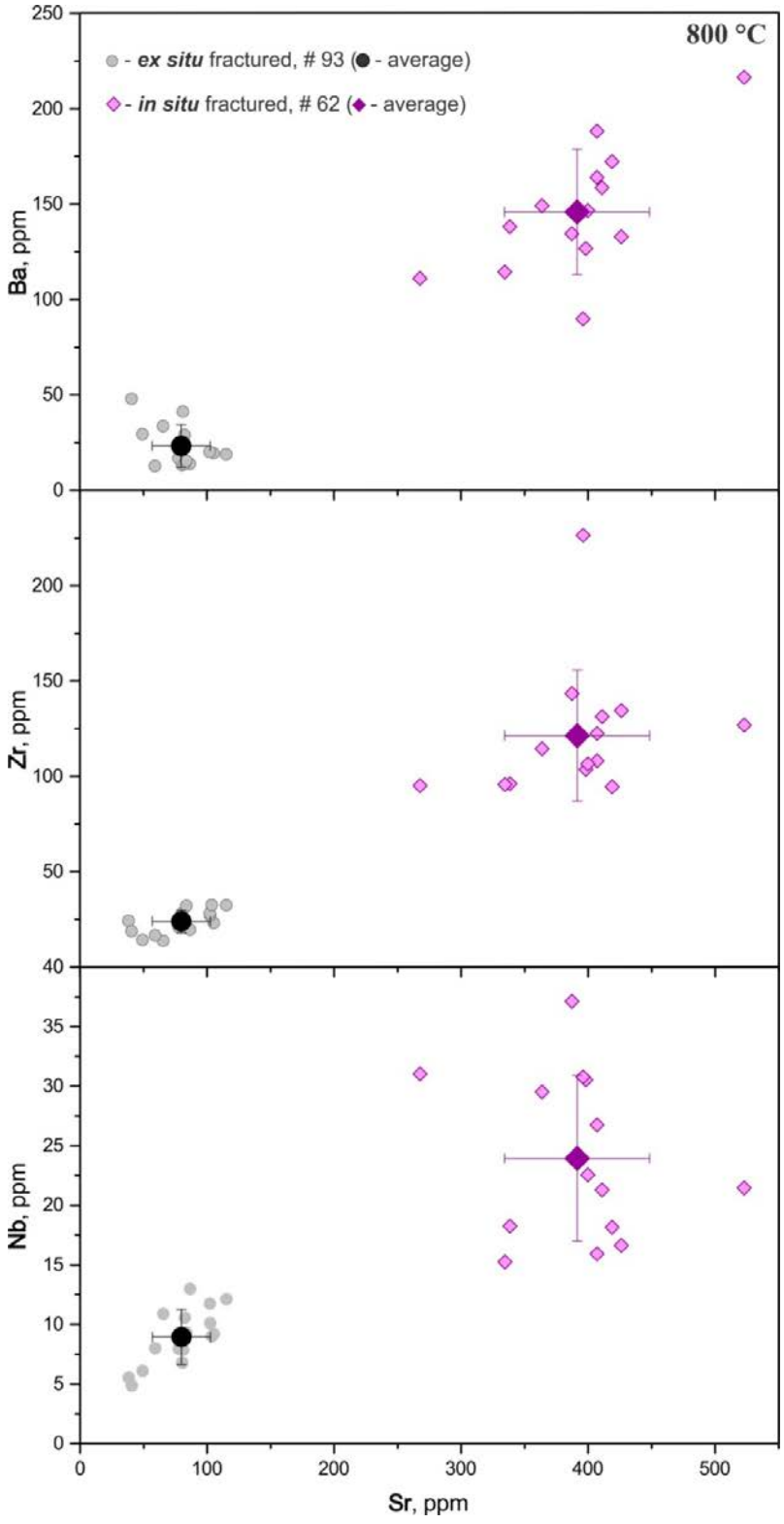

Figure 8

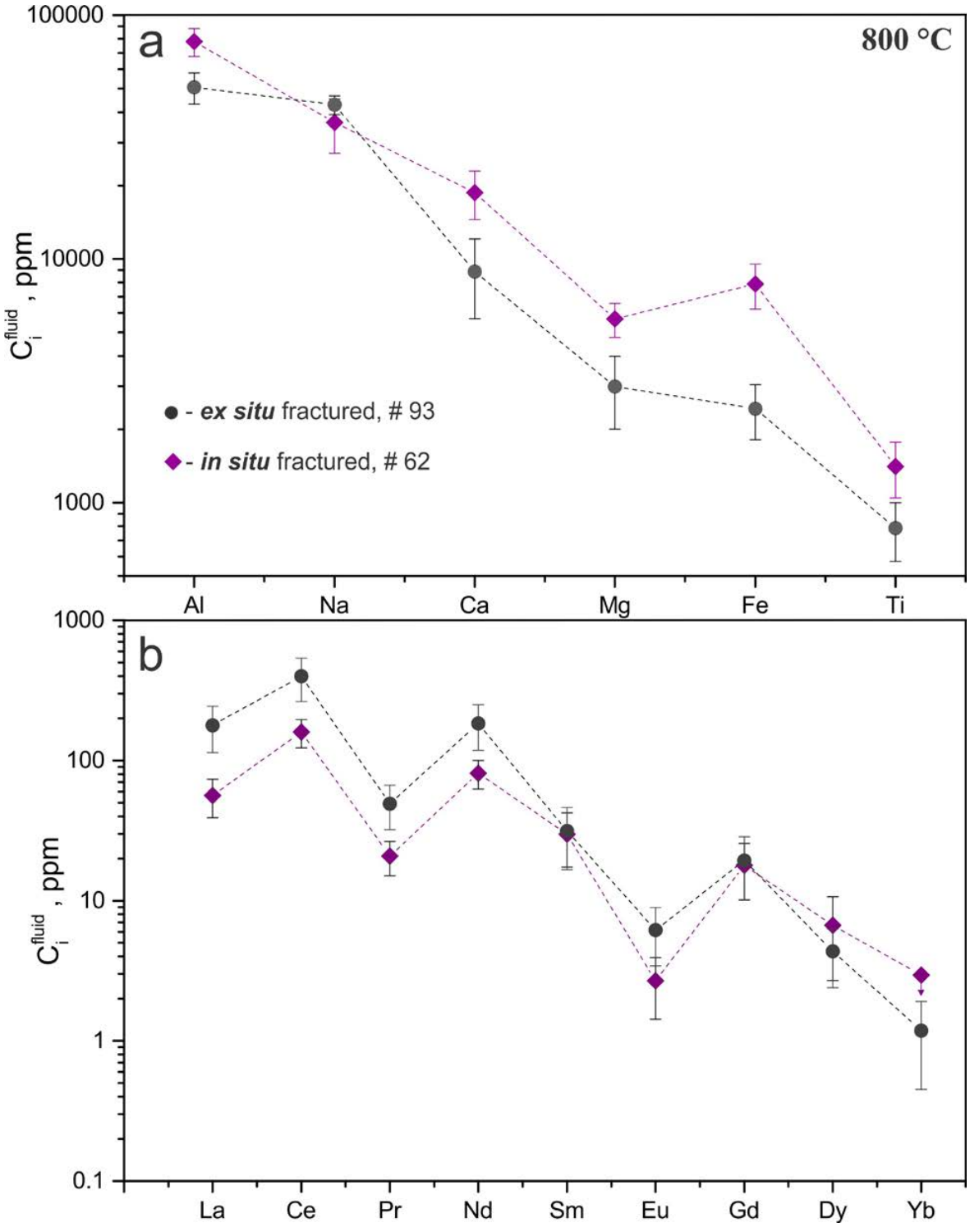
a
800 °C
100000
10000
1000
C_i^{fluid}, ppm
● - ex situ fractured, # 93
◆ - in situ fractured, # 62
Al
Na
Ca
Mg
Fe
Ti
b
1000
100
10
1
0.1
C_i^{fluid}, ppm
La
Ce
Pr
Nd
Sm
Eu
Gd
Dy
Yb

Figure 9